Materials Science & Engineering C 102 (2019) 405–414

Contents lists available at ScienceDirect

Materials Science & Engineering C

journal homepage: www.elsevier.com/locate/msec

Short communication

Graphene quantum dots unraveling: Green synthesis, characterization, radiolabeling with 99mTc, *in vivo* behavior and mutagenicity

Frederico Duarte de Menezes[a], Sara Rhaissa Rezende dos Reis[b], Suyene Rocha Pinto[b], Filipe Leal Portilho[b], Francisco do Vale Chaves e Mello[b], Edward Helal-Neto[b], Aline Oliveira da Silva de Barros[b], Luciana Magalhães Rebêlo Alencar[c], Alan Silva de Menezes[c], Clenilton Costa dos Santos[c], Aldilene Saraiva-Souza[d], Jamila Alessandra Perini[e], Daniel Escorsim Machado[e], Israel Felzenswalb[f], Carlos Fernando Araujo-Lima[f], Alyona Sukhanova[g,h], Igor Nabiev[g,h], Ralph Santos-Oliveira[b,i,*]

[a] Federal Institute of Education, Science and Technology of Pernambuco, Brazil
[b] Brazilian Nuclear Energy Commission, Nuclear Engineering Institute, Rua Helio de Almeida 75, Ilha do Fundão, CEP 21941-614 Rio de Janeiro, Brazil
[c] Federal University of Maranhão, Department of Physics, Avenida dos Portugueses 500, Vila Bacanga, CEP 65080-805 São Luís, Maranhão, Brazil
[d] Federal University of Piaui, Department of Physics, Bairro Ininga, CEP: 64.049-550 Teresina, Piaui, Brazil
[e] Research Laboratory of Pharmaceutical Sciences, Zona Oeste State University, Avenida Manuel Caldeira de Alvarenga 1.203, CEP 23070-200 Campo Grande, Rio de Janeiro, Brazil
[f] Department of Biophysics and Biometry, Rio de Janeiro State University, Boulevard 28 de Setembro, 87 Fundos, 4 ° Andar, CEP 20551-030 Rio de Janeiro, RJ, Brazil
[g] Laboratoire de Recherche en Nanosciences (LRN-EA4682), Université de Reims Champagne-Ardenne, 51, rue Cognacq Jay, 51096 Reims, France
[h] Laboratory of Nano-Bioengineering, National Research Nuclear University MEPhI (Moscow Engineering Physics Institute), KashirskoyeShosse 31, 115409 Moscow, Russian Federation
[i] Zona Oeste State University, Laboratory of Radiopharmacy and Nanoradiopharmaceuticals, Campo Grande, Rio de Janeiro, Brazil

A B S T R A C T

Graphene is one of the crystalline forms of carbon, along with diamond, graphite, carbon nanotubes, and fullerenes, and is considered as a revolutionary and innovating product. The use of a graphene-based nanolabels is one of the latest and most prominent application of graphene, especially in the field of diagnosis and, recently, *in loco* radiotherapy when coupled with radioisotopes. However, its biological behavior and mutagenicity in different cell or animal models, as well as the *in vivo* functional activities, are still unrevealed. In this study we have developed by a green route of synthesizing graphene quantum dots (GQDs) and characterized them. We have also developed a methodology for direct radiolabeling of GQDs with radioisotopes.Finally; we have evaluated *in vivo* biological behavior of GQDs using two different mice models and tested *in vitro* mutagenicity of GQDs. The results have shown that GQDs were formed with a size range of 160-280 nm, which was confirmed by DRX and Raman spectroscopy analysis, corroborating that the green synthesis is an alternative, environmentally friendly way to produce graphene. The radiolabeling test has shown that stable radiolabeled GQDs can be produced with a high yield (> 90%). The *in vivo* test has demonstrated a ubiquitous behavior when administered to healthy animals, with a high uptake by liver (> 26%) and small intestine (> 25%). Otherwise, in an inflammation/VEGF hyperexpression animal model (endometriosis), a very peculiar behavior of GQDs was observed, with a high uptake by kidneys (over 85%). The mutagenicity test has demonstrated A:T to G:C substitutions suggesting that GQDs exhibits mutagenic activity.

1. Introduction

Recently, the use of graphene based nanomaterials has increased worldwide. This new class of nanomaterials includes: graphene oxide (GO), nanographene oxide (NGO), reduced graphene oxide (rGO), graphene quantum dots (GQDs) and nano-reduced graphene oxide (nano-rGO) [1–3]. Among all the family of graphene nanomaterials, the graphene quantum dots (GQDs) is the most prominent one. They are nano-sized monolayers of graphene sheets with two-dimensional hexagonal lattice structure, which exhibits quantum confinement. The quantum confinement property is due the fact that at nanolevel the Broglie wavelength of an electron is comparable with the nanosystem itself. Since the quantum confinement is dependent on the size of the system, the GQDs may generate different photoluminescence (PL) spectra as a function of the size that is variable and can be tailored. Therefore, GQDs also have other properties that includes: i) size-tunable emission; ii) chemical and optical stability, iii) biocompatibility, iv) low toxicity, v) fluorescence emission, vi) NIR light absorption, vii)

* Corresponding author at: Brazilian Nuclear Energy Commission, Nuclear Engineering Institute, Rua Helio de Almeida, 75, Ilha do Fundão, Rio de Janeiro, Brazil.
E-mail address: roliveira@ien.gov.br (R. Santos-Oliveira).

https://doi.org/10.1016/j.msec.2019.04.058
Received 8 January 2019; Received in revised form 9 April 2019; Accepted 20 April 2019
Available online 24 April 2019
0928-4931/ © 2019 Elsevier B.V. All rights reserved.

photothermal properties and viii) typical Raman bands. Also, GQDs may be functionalized, especially due to its surface-volume ration and presence of sp^2 network that allows π–π stacking interactions. The whole of these properties can be used to enhance or complement GQDs properties to achieve synergic theranostic effects [4–8]. Thus, considering all the properties and features of GQDs, two major areas of interest where GQDs can be used are: bioimaging and drug delivery. The first one, use the luminescence to investigate and visualize biological matter, and the second one, use the surface-volume ratio and the ease to decorating feature. In both cases, a well understanding of the biological behavior is required in order to reach the best result.

Is important to notice that several studies discussing the biological behavior of GQDs were performed, many of them brought controversial data. A stinging clause among researchers leading with nanoparticles, involves the ability of nanoparticles to cross biological barriers such as blood-brain, placental and the cellular barriers in order to produce the desired effect. Is well known that nanoparticles may reach the target by two distinct mechanisms: transcellular and paracellular pathways. In the first case, nanoparticles cross the epithelial cell barrier *via* transcytosis. In the second, the nanoparticles pass through the tight junctions (TJs) [11,12]. In the case of GQDs, studies have reported that they are able to cross the cell membrane by a lipid raft-mediated transcytosis [13]. Therefore, despite the claim of low toxicity, some studies have reported that GQDs may induce oxidative stress in DNA level [9,10,14,15]. Although many studies regarding the GQDs biological behavior have been reported most of them were performed *in vitro* (cells), which differs drastically from the *in vivo* (animals). In this direction we developed, characterized, and evaluated *in vivo* the biological behavior of GQDs in two different models: healthy mice) and endometriotic rats (mimicking the disorganized tissue composition related to cancer proliferation – angiogenesis model). Also, we have performed the mutagenicity assay in order to better understand the oxidative stress mechanism involved in the exposition to QGDs.

2. Experimental

2.1. Development of graphene quantum dot

The procedure used to produce GQDs dispersions was based on an earlier published study [16]. Briefly, a graphite rod and a platinum wire were used as an anode and a cathode, respectively. The electrolyte used was prepared by mixing 63.5 mL of 0.2 M citric acid with 36.5 mL of 0.2 M sodium citrate to obtain 100 mL of electrolyte. The electrochemical process was conducted at a constant current of 190 mA for 24 h using an ICEL PS-1500 adjustable power supply. After the oxidation electrolysis, the dispersion obtained was filtered to remove large particles. The filtered suspension was dried at 60 °C to reduce the volume of the dispersion to 10 mL. Finally, 50 mL of ethanol was added to the dispersion, and the upper phase corresponding to purified GQDs was collected. The purified GQDs were dried at 60 °C until use.

2.2. Size determination by dynamic light scattering

The size distribution, mean size, and polydispersity index (PDI) of the GQDs were determined by dynamic light scattering (DLS) using a Zetasizer Nano ZS equipment (Malvern Instruments, UK). The measurements were performed in triplicate at 25 °C and a laser incidence angle relative to the sample of173° using a 12-mm^2 quartz cuvette. The mean ± standard deviation (SD) was assessed. In order to evaluate the problems related to graphene DLS analysis, an ultra-diluted solution (1:400.000) in Milli-Q water was used.

2.3. Raman analysis

The Raman spectra were obtained using a Horiba-Jobin-Yvon triple spectrometer (model T64000). The instrument was equipped with a confocal attachment and a liquid-N_2-cooled charge coupled device (CCD) detector. For excitation, a green line (532.0 nm) from a solid-state laser (LAS-532-100-HREV) operating at 14 mW was employed. The light was focused on the sample using an Olympus microscope with an MPLN 100× objective lens. The spot of the scattered light was limited by the confocal attachment. The spectra were acquired in two ways: (i) at different points on the sample surface and (ii) by varying the position along the vertical direction centered on a particle.

2.4. Atomic force microscopy

2.4.1. Topography and phase images

Atomic force microscopy (AFM) experiments were performed with a Multimode 8 (Bruker, Santa Barbara) using the Nanoscope Analysis 1.50software (Bruker) in the tapping mode (intermittent contact) for acquisition of topographic and phase images in order to determine the diameter, height, and phase composition of the particles. Experiments were performed with a cantilever spring constant of 0.24 N/m and a nominal tip radius of 2 nm. The particle solutions were diluted to a concentration of approximately $10^9$to 10^{10}particles per 1 cm^3. The solutions were dropped in fresh cleaved mica and left to dry in a vacuum chamber protected from contamination. The experiment was performed with a scan resolution of 256 × 256 lines and a frequency of 0.5 Hz.

2.5. Optical properties

The optical properties of the purified GQD dispersion were estimated using absorbance and fluorescence spectroscopy by means of a Cary 60 UV–Vis (Agilent) and an Ocean Optics HR2000 spectrophotometers, respectively. For the fluorescence analysis, the sample was excited with a LED at an emission wavelength of395 nm.

2.6. Powder X-ray diffraction

The characteristics of GQDs were estimated by powder X-ray diffraction (PXRD). PXRD measurements were done using a Bruker AXS D8 Advance diffractometer equipped with a CuKα radiation source and operating at 40 mA,/40 kV. PXRD measurements were performed in high angle (2θ = 15–68°) and low angle (2θ = 1.3–8.3°) ranges.

2.7. Labeling with ^{99m}Tc

The labeling process was done using 150 μg of GQDs incubated in 100 μL of stannous chloride ($SnCl_2$) solutions (80 μL/mL) (Sigma-Aldrich) for 20 min at room temperature. Then, this solution was incubated with 100 μCi (approximately 300 μL) of technetium-99 m for another 10 min in order to label the GQD structures.

2.8. Quality control of the labeled GQDs with ^{99m}Tc

In order to confirm the efficiency of the labeling process, Radio Thin Layer Chromatography (RTLC) was done using Whatman paper no.1 and 2 μL of the ^{99m}Tc-GQDsin acetone (Sigma-Aldrich) as a mobile phase at time points of 2 and 4 h. The radioactivity of the strips was verified in a γ-counter (Perkin Elmer Wizard® 2470, Shelton, CT, USA). The RTLC was performed in triplicate for each time point.

2.9. Animal experimental design

The GQDs were analyzed under two distinct conditions. The first one we evaluated the biological behavior of GQDs in healthy Balb/C mice. The second one we evaluated the biological behavior of the GQDs in rats inducted with endometriosis. Is important to notice that we have used endometriotic rats in order to evaluate the influence of angiogenesis in GQDs nanoparticles tissue deposition. The endometriosis model is a general method that mimics the basal inflammation and the

formation of new vessels in tumor without the interference of any specific oncogenesis [17] *Healthy Animals.*

2.9.1. Healthy animals

Animals (male Balb/c mice, $n = 6$) were treated in accordance with the protocols no. 182/2017 approved by the Institutional Animal Care and Use Internal Review Board of the Institute of Energy and Nuclear Research. The mice received water and food *ad libitum* and were used after reaching maturity at 6 weeks of age.

2.9.2. Angiogenesis model

2.9.2.1. Surgical induction of endometriosis. The animals ($n = 6$, female Wistar rats) were treated in accordance with protocols approved by the Institutional Animal Care and Use Internal Review Board of the Federal University of Rio de Janeiro (IBCCF-009/2008). The endometriosis model was established as previously described [18]. In brief, the abdominal cavities of six female Wistar rats were opened through a 3-cm midline incision to expose the uterus. One uterine horn was ligated at both the uterotubal junction and the cervical end and was removed. The segment was placed in phosphate-buffered saline at 37 °C, split longitudinally, and 5 × 5 mm pieces were sectioned. These explants were then anchored onto the peritoneum on the right side of the ventral abdominal wall by non-absorbable polypropylene sutures (Prolene 6–0; Ethicon, Piscataway, NJ, USA). The abdomen was closed, and the animals were allowed to recover from anesthesia. A total of 6 mice of this group were used in this study.

2.10. Histology and immunohistochemistry

In order to confirm the endometriosis formation both histology and immunohistochemistry of lesions were performed. In brief, formalin-fixed tissues were paraffin-embedded and cut into 4-μm-thick sections. Harris' hematoxylin and eosin staining was performed, and the tissues were examined microscopically for the presence of histological hallmarks of endometriosis. The other paraffin-embedded tissue sections were placed on poly-L-lysine-treated slides and kept at room temperature. After dewaxing, the sections were treated with a solution of 3% H_2O_2 in 0.01 mol/L phosphate-buffered saline (PBS), pH 7.5, to inhibit endogenous peroxidase activity. The slides were then immersed in 0.01 M citrate buffer (pH 6.0) and heated in a microwave oven for 15 min to retrieve masked antigens. To reduce nonspecific antibody binding, the sections were then incubated with PBS containing 4% Molico®milk powder and 5% bovine serum albumin for 30 min. The sections were incubated with polyclonal anti-VEGF antibodies (Abcam, ab46154) ata dilution of 1:200. The slides were incubated overnight and then were washed three times in PBS and incubated for 1 h with compatible secondary antibodies (Anti-rabbit, 1:100, Vector Laboratories, BA-1000). The reaction was revealed with DAB (Sigma-Aldrich). Images were obtained using an Olympus BX60 microscope.

2.11. Biodistribution

For the biodistribution studies, 3.7 MBq/0.03 mL of GQDs labeled with ^{99m}Tc was injected by the retro-orbital route for evaluating the systemic behavior in two groups: group 1 consisted of healthy animals ($n = 6$), and group 2 animals with endometriosis (n = 6). Briefly, the animals were anesthetized intramuscularly with a mixture of 10% Ketamine and 2% Xylazine. Then, ^{99m}Tc-GQDs were administered by retro-orbital injection. Two hours post-injection, both groups were euthanized by asphyxiation (CO_2chamber), and the organs of interest (the heart, brain, stomach, intestine, bladder, kidney, lung, liver, spleen, blood, and affected endometrium) were immediately dissected out and weighted for quantitative estimation of gamma counts using a gamma counter (Perkin Elmer, Wizard® 2470). The results were expressed as percentage of injected dose per organ (%ID/g).

2.12. Mutagenicity

2.12.1. Salmonella/microsome mutagenicity test

The traits of *Salmonella enteric* serovar Typhimurium standard strains TA98, TA100, and TA102 were phenotypically checked immediately before the use in the experiments. The test tube contained a mixture of 100 μL of one of the eight concentrations of GQDS, 500 μL sodium phosphate buffer (27.6 g/L $NaH_2PO_4{\cdot}H_2O$ and 28.4 g/L Na_2HPO_4; 0.2 M, pH 7.4) and 100 μL of the bacterial suspension (2×10^9 cells/mL). After a pre-incubation for 20 min with stirring, at 37 °C, 2 mL of top agar (7 g/L agar; 5 g/L NaCl; 0.0105 g/L L-histidine; 0.0122 g/L biotin; pH 7.4, 45 °C) was added to the test tube, and the final mixture was poured onto a Petri dish with minimal agar (15 g/L agar, Vogel-Bonner E medium 10× (10 g/L $MgSO_4{\cdot}7H_2O$; 100 g/L $C_6H_8O_7{\cdot}H_2O$; 500 g/L K_2HPO_4; 175 g/L $Na(NH_4)HPO_4{\cdot}4H_2O$) containing 20 g/L glucose. This final mixture was incubated at 37 °C for 72 h, and His^+ revertant colonies were counted. The sample was considered positive for mutagenicity when a significant response to the analysis of variance (ANOVA) ($p \leq 0.05$) and reproducible positive dose-response curve were found. All the experiments were done in triplicate and repeated at least twice [19,20].

2.13. Statistical analysis

The statistical analyses were performed using the GraphPad Prism 6.0 software (GraphPad Software, Inc.). Results are shown as the mean ± standard deviation (SD). To determine statistically significant differences between groups, normal distribution was assumed and one-way ANOVA was used. The differences were considered statistically significant at $p < 0.05$.

3. Results and discussion

3.1. Development of graphene quantum dot

There are several ways to produce GQDs. These methods are divided into two categories: i) top-down strategy and ii) bottom-up strategy [21]. Among these methods can be highlighted: electron beam lithography, hydrothermal route, acidic exfoliation, chemical oxidation (oxidative cleavage), chemical ablation, Laser ablation method, carbonization of organic precursors, solution chemistry, solvothermal synthesis, ultrasonic and irradiation method [21,22]. The electron-beam lithography, laser ablation, ultrasonic method and chemical ablation are limited by the requirement for special equipment, extremely expensive raw materials and low yield. Also the acid exfoliation, chemical oxidation and solvothermal synthesis requires high amounts of chemical solvents as H_2SO_4 and HNO_3 (sulfuric acid and nitric acid respectively). The hydrothermal or electrochemical strategies can be used, but these methods are limited to GO as starting material, and also require a series of chemical treatments which typically take several days and involve lots of chemical reagents. Nevertheless, these methods offered the GQDs with only one emission color (blue or green luminescence) and with limited size [22–24]. A green and environmentally friend route was described by Bayat and Iranizad [25]. In this methodology a low-cost and high-yield green-photoluminescent single-layer GQDs were synthesized with only deionized water and glucose as a precursor. But the size variation was limited and not adequate for biological application [26,27]. Thus, in comparison with all the other methods, including a green route, the electrochemistry methodology described in this study, was capable to produce organic solvent-free and size tailoring GQDs that are well-designed for biological application.

3.2. Size determination by dynamic light scattering

The DLS (Fig. 1) uses the Stokes-Einstein equation, which presumes a spherical shape for the nanoparticles in order to deduce the particle

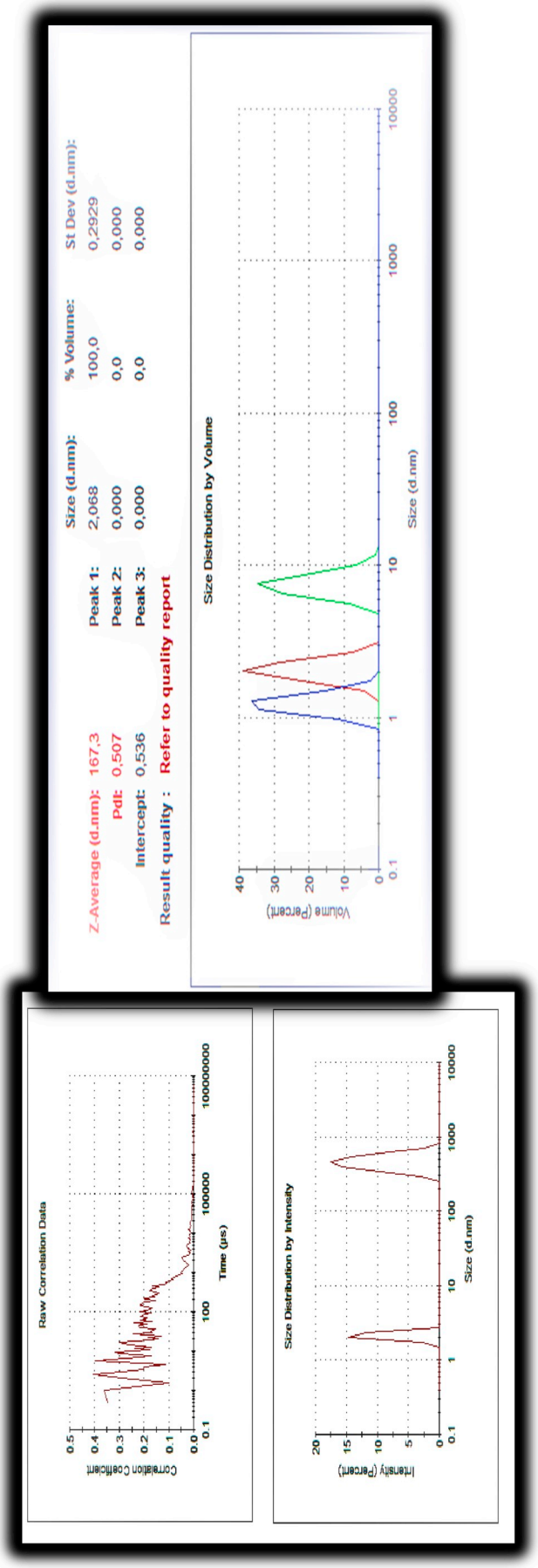


Fig. 1. Dynamic light scattering analysis of the ultra-high-diluted sample (1:400.000) of graphene quantum dots (GQDs). The mean size was of 167.3 nm.

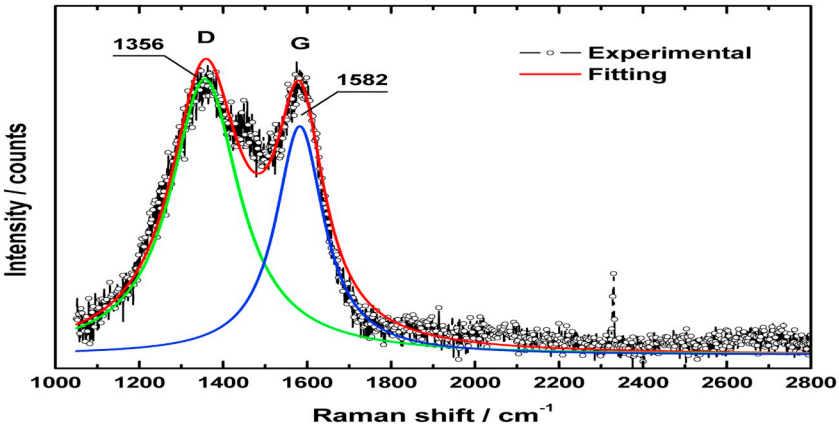


Fig. 2. Raman Analysis showing the spectrum of GO, where the in-phase vibration (G band) of GO is ~1600 cm-1 and the disorder band (D band) of GO is at ~1360 cm. Is possible to observe the intense bands D and G at 1356 and 1582 cm-1, respectively, with the intensity ratio between ID/IG of the D and G peak relatively high (~ 1.2), corroborating the purity of the graphene. Also, is not observed a peak at ~ 2690 cm-1, which indicates the formation of the 2D structure, corroborating in this case, the formation of the Graphene Quantum Dots.

radius and then calculate the translational diffusion constant of the particles. However, GQDS have no rotational symmetry; hence, the DLS analysis would yield two translational diffusion coefficients and also the rotational diffusion coefficient [28,29]. Therefore, assuming that the diameters of our GQDs were larger than the thickness of the 2D flakes, the result of the DLS is near the real size. In this case, and assuming these inferences, our GQDs showed a size of 167.3 nm. The PDI value of 0.507 is not relevant, considering the epigraph, because graphene is a 2D structure with no rotational symmetry.

3.3. Raman analysis

The Raman spectra revealed the presence of bands at ~1360 cm-1 and ~1600 cm-1 (Fig. 2), which are the D and G characteristic bands of graphene, associated with disorder or defects in the lattice and C—C vibrations, respectively. Although the samples had been washed with Milli-Q water to minimize the influence of citrate on Raman spectroscopy measurements, bands attributed to the substrate on which the sample was deposited, or remnants of the quantum dots preparation route, such as citrate, can also be observed.

3.4. Atomic force microscopy

The atomic force microscopy (AFM) results are showed in Fig. 3. According to the data analysis, the average diameter of the GQDs ranged in the interval of 160–280 nm, while the most frequent heights were about 5 nm. The roughness was very low, with an Rq of 4.58 nm and Ra of 3.42 nm.

3.5. Powder X-ray diffraction

The powder X-ray diffraction analysis corroborated the formation of GQDs, as seen in Fig. 4. A great number of other peaks are also seen. All those peaks are due the presence of citrate. Citrate was used in the preparation of GO/GQDs and was detected by the PXRD analysis (Table 1). The GQDs has a broad peak close to $2\theta = 25^{o}$, that could not be properly seen due the citrate phase, which has two intense peaks in the same region. However, the Raman measurement of the purified sample has confirmed the presence of GQDs.

We decided to keep the citrate in the sample considering its antioxidant properties that would be relevant for a pharmaceutical/biological application of these GQDs [30].

3.6. Optical properties of graphene QDs

The optical properties of GQDs are showing in Fig. 5.

The results showed a maximum absorbance at 265 nm, and the fluorescence emission was observed in the region between 500 and 550 nm, corroborating the photoluminescence properties [31,32].

3.7. Radiolabeling

3.7.1. Radiochemical purity of the GQDs nanoparticles

A simple, rapid, efficient and direct method for labeling GQDs with ^{99m}Tc was developed. The labeling efficiency of the ^{99m}Tc-GQDs nanoparticles was assessed by RTLC. In RTLC, using acetone as the solvent, free ^{99m}Tc moved with the solvent front, while ^{99m}Tc-GQDs nanoparticles remained at the spotting point. The radiochemical purity was found to be over 97% for as long as 4 h without any significant changes during the incubation ($p > 0.05$) (Table 2).

The stability of GQDs with ^{99m}Tc for4 hours and the high yielding percentage proved that the labeling methodology was efficient and safe, and a similar methodology could be used in order to introduce other radioisotopes for therapeutic purposes too.

3.8. Biodistribution

3.8.1. Healthy animals

The results of the GODs biodistribution in healthy animals are showed in Fig. 6.Is possible to observe that the ^{99m}Tc-GQDs were uptake by liver (23.14%) and spleen (0.61%). Considering that nanoparticles are easily recognized by the mononuclear phagocytic system (MPS) represented mainly by the liver and spleen [33], this result is not surprising. However, the amount of GQDs uptake was very small, which suggests an alternative pathway of nanoparticles avoiding the MPS. The amounts taken up by the small intestine (29.35%) and large intestine (5.85%) apparently confirm enterohepatic excretion of ^{99m}Tc-GQDs nanoparticles taken up by liver.

However, the uptake by the stomach (8.25%) needs also be considered. The presence of GQDs in the stomach, considering that retroorbital injection was used, may be explained by assuming that some of the ^{99m}Tc-GQD reach a colloidal state, as observed with ^{99m}Tc-Sn(OH)$_n$ colloid, and, for that reason, are taken up by the stomach [34]. The data on the kidney excretion are important. Both kidneys (Σ 24.97%) uptake ^{99m}Tc-GQDs, and the result of clearance is confirmed by the presence of ^{99m}Tc-GQD nanoparticles in the bladder (4.27%), which agrees with the data of Kurantowicz et al. [35]. Although Kurantowicz et al. [35] had studied smaller GO (8-25 nm) is well known that glomerular capillary pores, known as fenestrae are 60–100 nm wide. Nevertheless, biophysical studies demonstrate that fenestrated and nonfenestrated capillaries have comparable permeabilities to macromolecules [36,39]. The very low uptake in the brain corroborates the safety aspect regarding the blood-brain barrier (BBB). In addition, the low blood content of GQDs indicates poor binding with blood proteins, such as albumin. This may be explained by the fact that GQDs nanoparticles have a 2D geometry [38]. The 2D geometry may lead to an erratic spatial conformation, which causes an allosteric impediment and, consequently, difficulty in binding with blood proteins.

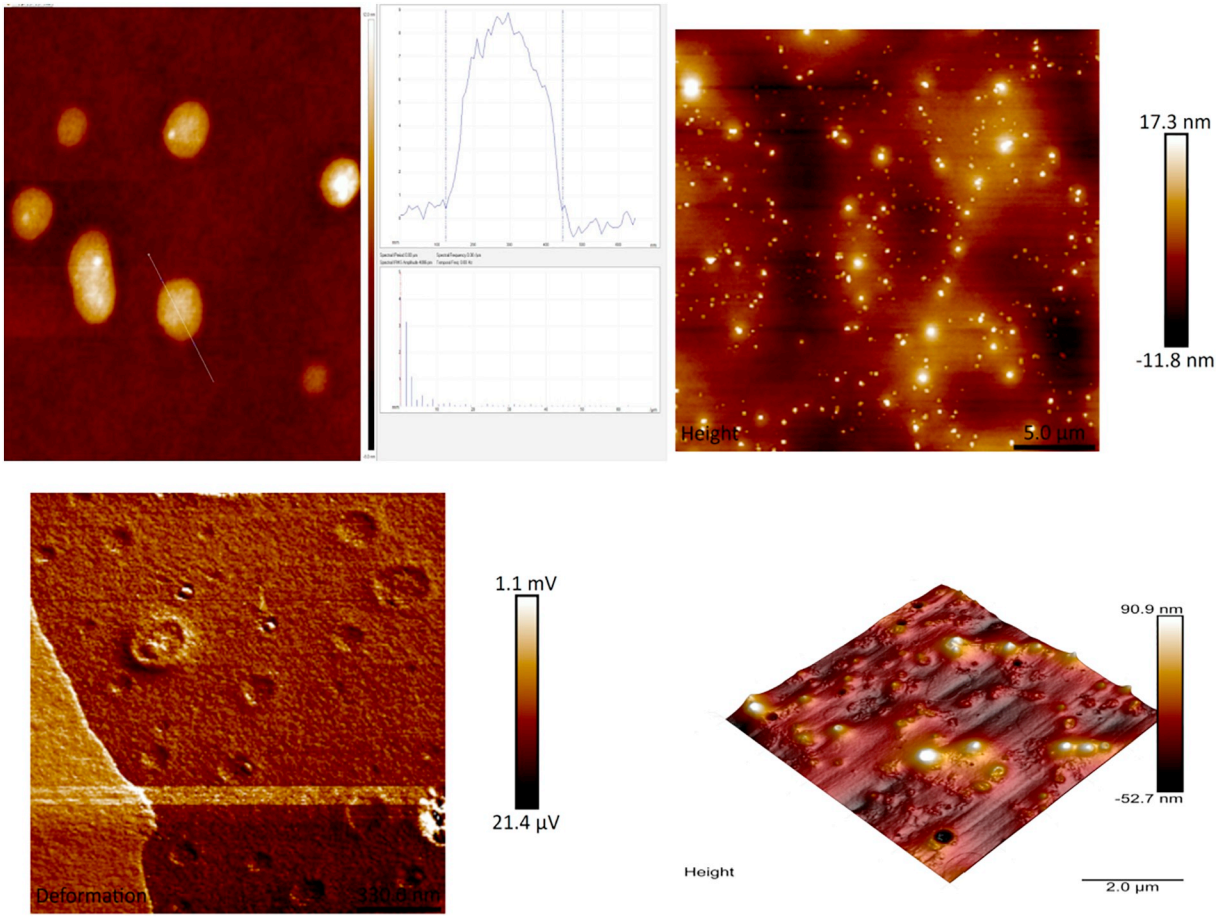


Fig. 3. Atomic force microscopic analysis of the graphene quantum dotsshowing their size distribution (160-280 nm). A good homogeneity and the height of the nanoparticles showing a low roughness and the presence of coverslips are seen.

3.8.2. Angiogenesis model

The angiogenesis model using the endometriosis induction was confirmed by histology and macro-analysis of the animals (Fig. 7). In all animals, endometriosis was confirmed. In addition, the VEGF immunoreactivity observed as the expression of mRNA encoding VEGF was tested, and the results corroborated the high level of VEGF in inducted animals (Fig. 7).

In order to evaluate the possible interaction between the GQDs and the neoangiogenesis environment closely associated with the tumor

Table 1
PXRD analysis of GQDs showing the presence of citrate in the graphene oxide sample due the fabrication route used.

Visible	Ref. code	Score	Compound name	Scale factor	Chemical formula
*	00-016-1180	65	Disodium hydrogen citrate dihydrate	1.195	$C_6H_6Na_2O_7{\cdot}2H_2O$

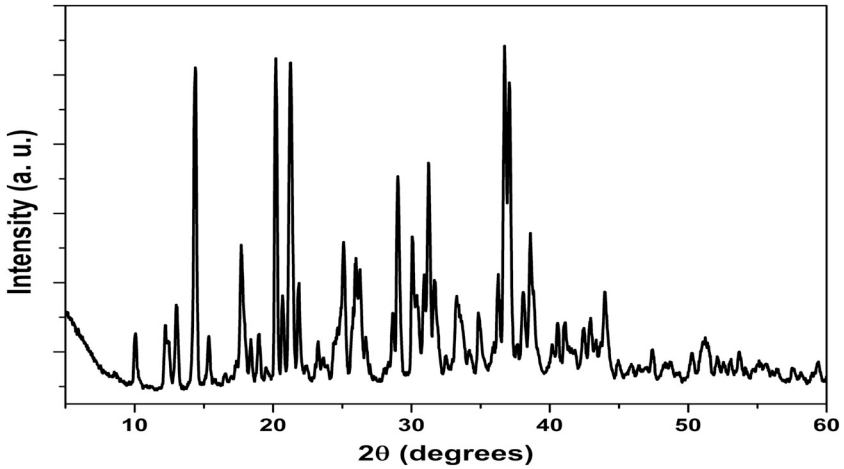


Fig. 4. The powder X-ray diffraction (PXRD) analysis of sample showing the formation of graphene peak at 2θ = 10, as also the presence of citrate.

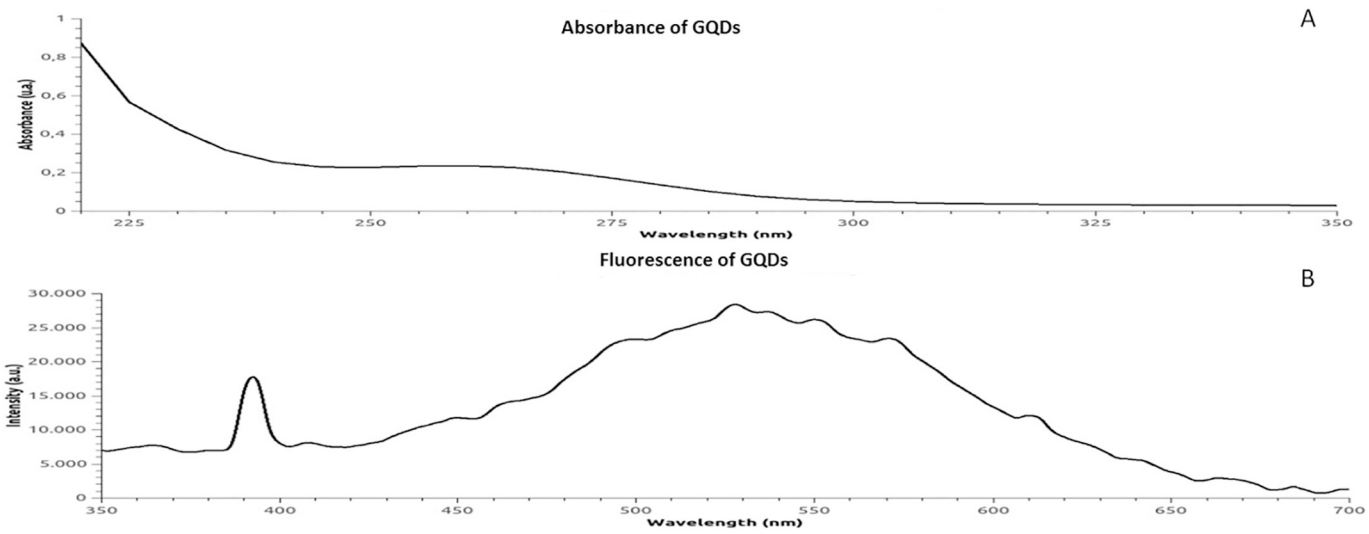


Fig. 5. The optical properties of the graphene quantum dots. Panel A shows absorption spectrum of GQDs with a maximum at 265 nm and the Panel B shows fluorescence spectrum with the maximum around 530 nm.

Table 2
Radiochemical purity (%) of ^{99m}Tc GQDs in 2 and 4 h.

Time (hours)	Radiochemical purity (%)
2	97.70 ± 0.2
4	98.72 ± 0.13

growth, we evaluated the ^{99m}Tc-GQDs biodistribution in the angiogenesis model (endometriosis induction). The results are shown in Fig. 8.

The results showed that the presence of VEGF and a whole new vascularization zone changed the biological behavior of the ^{99m}Tc-GQD. Endometriosis increased the renal clearance (47,78% and 41,51% left and right kidney respectively). Although no information regarding the correlation between endometriosis and augmented renal clearance has been found, which could justify these data, we found that some clinical conditions, such as inflammation, and severe postsurgical conditions in rats, can increase the glomerular filtration rate (GFR) and the renal clearance itself [37]. The uptake in the stomach (5,78%) was almost half of that in healthy animals. The reduced uptake in the intestine (2,47% and 3,31% small and large intestine respectively) may have been correlated with the low uptake in the liver, which confirms the enterohepatic elimination observed in the healthy animals. No information was found on correlation between the liver function and endometriosis. On the other hand, itis known that a healthy liver is also a site of complex immunological activity mediated by a diverse immune cell repertoire, as well as non-hematopoietic cell populations. In a non-diseased liver, metabolic and tissue remodeling functions require elements of inflammation [38]. Therefore, we believe that endometriosis associated with the entire health condition of the body could be responsible for reducing the liver function, and for the lower uptake in the liver observed in endometriotic rats. The uptake in the endometriotic lesion is an important finding. A negligible amount of ^{99m}Tc-GQDs was found in the endometriotic lesion, which corroborates that the whole angiogenesis process with a whole new vascularization area did not interfere with the accumulation of ^{99m}Tc-GQDs in this zone. This data corroborates the use of GQDs nanoparticles with especial attention for tumor imaging and/or drug delivery template, as stated by Ren et al. [40]. The negligible results confirm that the use of the type of nanoparticles may be tailored and functionalized for this kind of purpose.

Finally is important to notice that in both cases (healthy and inducted, such as male and female animals) no aberrant tissue deposition has been noticed, which corroborates the use aspect related to GQDs as also confirmed by Zhang et al. [41].

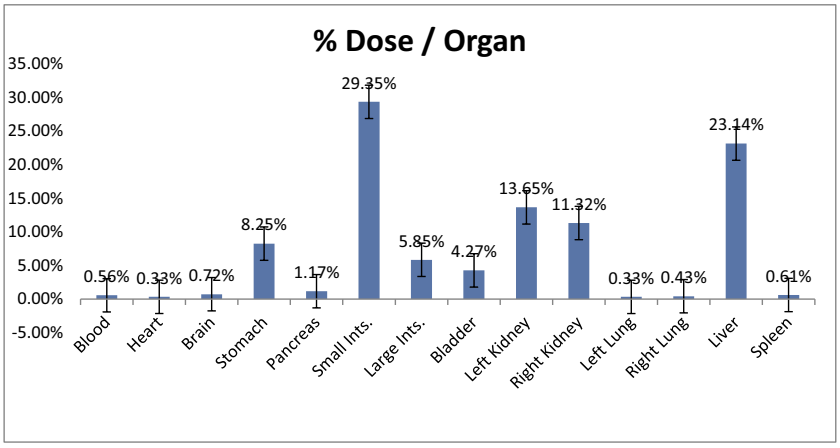


Fig. 6. Biodistribution of ^{99m}Tc-GQDin healthy animals (Balb/c mice) 2 h after retro-orbital injection.

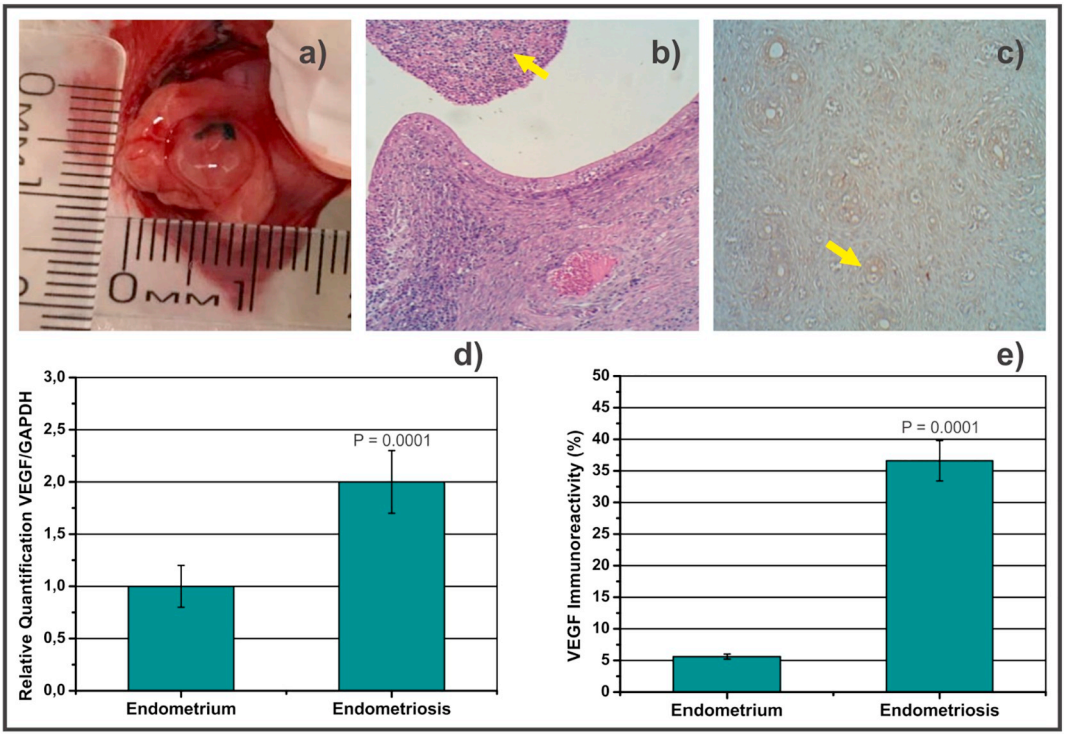


Fig. 7. (A, B) Morphological characteristics of the experimental mice endometriosis model showing the eutopic endometrium 15 days after induction. Histologically, the endometriotic tissues were similar to the eutopic endometrium. (C) VEGF immunodistribution of eutopic endometrium. (D) Morphometric analysis confirmed the increase in the VEGF level in the endometriotic lesions compared with the eutopic endometrium. (E) The expression of mRNA encoding VEGF also showed that the levels of VEGF were significantly higher in endometriosis than in the eutopic endometrium.

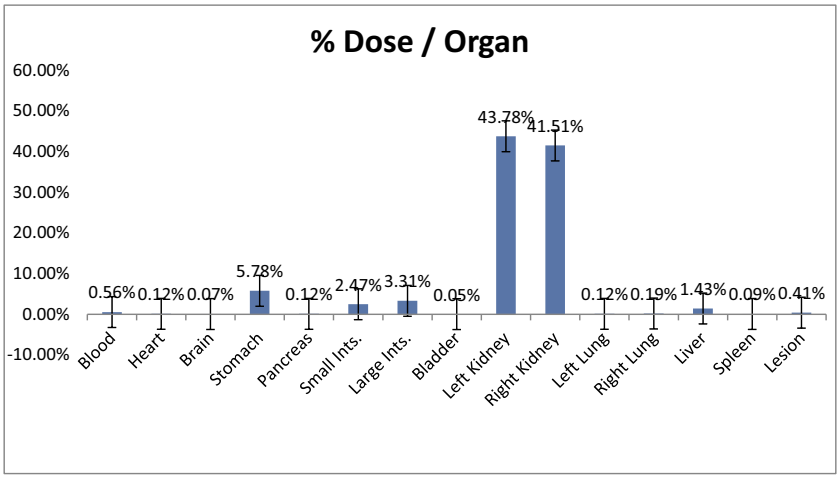


Fig. 8. Biodistribution of ^{99m}Tc-GQDs in inducted animals with endometriosis 2 h after the injection, mimicking a high expression of VEGF and reflecting the behavior of GQDs in the environment. In this figure, lesion means the endometriotic region, the highest zone of expression of VEGF.

3.9. Mutagenicity

According to the Organization for Economic Cooperation and Development (OECD), all products intended for human use should be evaluated regarding toxicological aspects. It is recommended that at least two *in vitro* toxicological tests be carried out before proceeding to *in vivo* experimentation [42]. In general, the preliminary toxicity assessment using the Ames test, which detects point mutations in the DNA sequence, is recommended for any chemical substance used for human or animal health. In the present study, the *Salmonella*/microsome assay was used to screen the GQDs nanoparticles mutagenicity, following recommendations of the OECD, guideline 471, using the TA98, TA100, TA102, and TA104strains, in the absence of metabolic activation (Fig. 9).

As shown here, no frame shift mutagenic activity (TA98 strain) or mutagenicity causing G:C to A:T substitution (TA100) was observed. It was possible to observe the cytotoxic profiles of the GQDs for those strains, mainly at higher concentrations. On the other hand, the strains which detect A:T to G:C substitution (TA102 and TA104) displayed a clear dose-response profile, suggesting that GQDs induced mutations. This pair of strains can detect oxidative DNA damage, and they differ from each other in the proficiency of nucleotide excision repair (NER), where TA102 expresses the *uvrB* gene, while TA104 does not express it [43]. In this sense, many studies have shown that oxidative stress is one

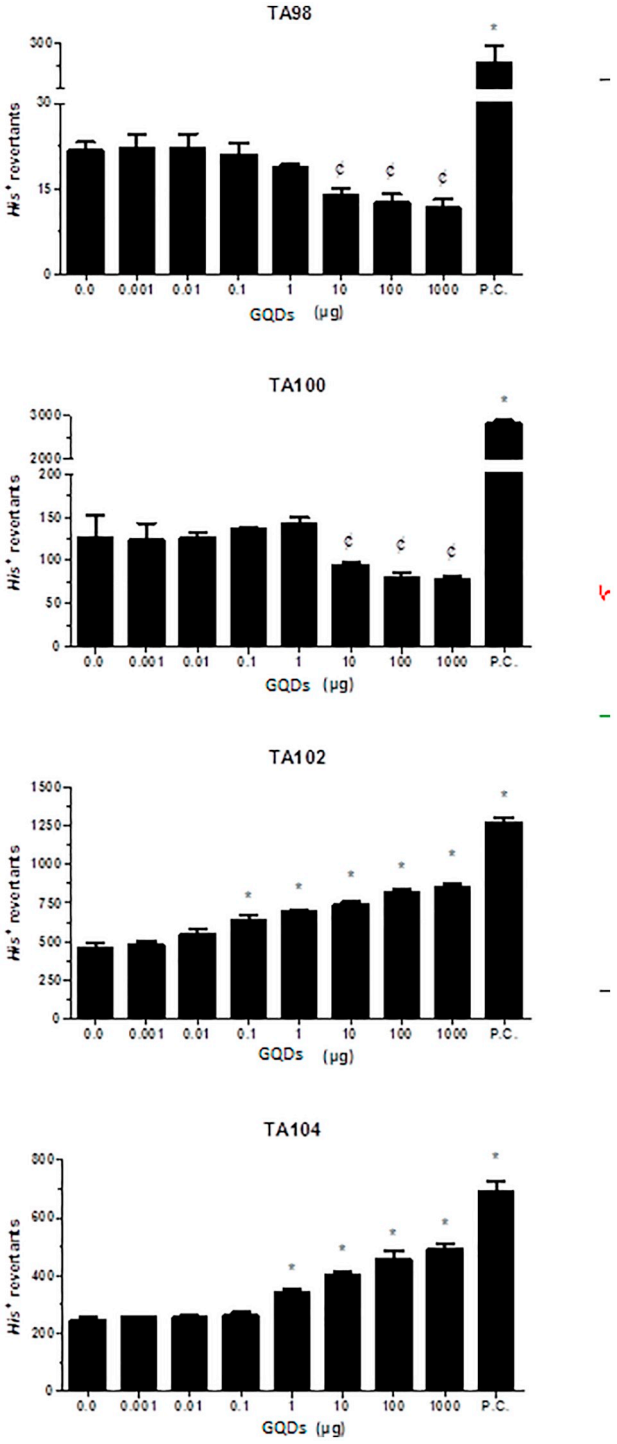


Fig. 9. Revertant colonies of the TA98, TA100, TA102, and TA104 strains of the*Salmonella enterica* serovar Typhimurium *His*$^+$in the Ames test after incubation with graphene quantum dots. *, Differencefrom the negative control; ¢,cytotoxic;one-way ANOVA followed by Tukey's *post hoc* test ($p < 0.05$). Positive controls (P.C.) were 4-nitroquinoline-N-oxide (1.0 µg/plate) for TA98; sodium azide(1.0 µg/plate) for TA100; mytomicin-C (0.5 µg/plate) for TA102; and methyl methanesulphonate (250 µg/plate) for TA104.

of the mechanisms involved in the toxic effects of the carbon nanomaterial [44]. We observed a discrete increase inTA102 *His*$^+$revertants compared to TA104 at a dose of 0.1 µg, which suggests that, after a DNA lesion, NER repair mechanisms can favor translesion DNA repair [45], resulting in point-mutated sequences and enhancing the GQDs mutagenicity, corroborating the literature information.

4. Conclusion

In general the results sustained the use of GQDs nanoparticles for human use. The results have shown that, despite some interference with the DNA function, especially related to the oxidative stress, the GQDs nanoparticles seem to be safe. A distinct behavior has been noticed in both models studied, with an augmented renal clearance in animals with endometriosis, which has been related to the increased glomerular filtration rate under this condition. Also has been observed a reduced uptake by the stomach and a very limited uptake by the mononuclear phagocytic system. Under normal conditions (healthy animals) a ubiquitous biodistribution has been observed. The main information relies in the negligible tissue deposition in brain and a possible enterohepatic pathway. The presence of oxygen functional groups imparts high water solubility, which is quite desirable for biomedical application. Finally, the synthetic way to obtain the GQD is an important factor. The classical Hummer's method and its derivations use, for example, hazardous reagents such as oxidant salts and acids making these routes unfavorable for producing GQDs for biomedical application. In this study we used a green route to produce a well-stable GQDs that could be used in animals and which use could translated to humans.

Conflict of interest

The authors state that they have no conflict of interest.

Acknowledgements

The authors would like to thank CAPES (Brazil) and CNPq (Brazil) for the financial support of this research. Also, the Russian Science Foundation, contract number 17-15-01533. I.N. acknowledges support of the Agence Nationale de Recherche through the ERA-NET project ICENAP.

References

[1] Y. Wu, H. Zhang, A. Pan, Q. Wang, Y. Zhang, G. Zhou, L. He, White-light-emitting melamine-formaldehyde microspheres through polymer-mediated aggregation and encapsulation of graphene quantum dots, Adv Sci 6 (2) (2019 Jan 23) 1801432.
[2] T. Viseu, C.M. Lopes, E. Fernades, et al., A systematic review and critical analysis of the role of graphene based nanomaterials in cancer theranostics, Pharmaceutics 10 (4) (2018) 282 Dec.
[3] H. Shen, L. Zhang, M. Liu, Z. Zhang, Biomedical applications of graphene, Theranostics 2 (3) (2012) 283–294.
[4] Yim SG, Kim YJ, Kang YE, Moon BK, Jung ES, Yang SY. Size fraction of fluorescent graphene quantum dots using a cross-flow membrane filtration system. Nanomaterials. 2018 Nov 21;8(11). (pii: E959).
[5] J. Wu, P. Wang, F. Wang, Y. Fang, Investigatioion of the microstructure of graphene quantum dots (GQDs) by surface-enhaced raman spectroscopy, Nanomaterials 8 (10) (2018) Oct 22. (pii: E864).
[6] T. Gao, X. Wang, L.-Y. Yang, H. He, X.-X. Ba, J. Zhao, F.-L. Jiang, Y. Liu, Red, yellow, and blue luminescence by graphene quantum dots: syntheses, mechanism, and cellular imaging, ACS Appl. Mater. Interfaces 9 (2017) 24846–24856.
[7] K.L. Schroeder, R.V. Goreham, T. Nann, Graphene quantum dots for theranostic and bioimaging, Pharm. Res. 33 (10) (2016) 2337–2357 Oct.
[8] W. Chen, G. Lv, W. Hu, D. Li, S. Chen, Z. Dai, Synthesis and applications of graphene quantum dots: a review, Nanotechnol. Rev. 7 (2018) 157.
[9] Y. Chong, Y. Ma, H. Shen, X. Tu, X. Zhou, J. Xu, J. Dai, S. Fan, Z. Zhang, The in vitro and in vivo toxicity of graphene quantum dots, Biomaterials 35 (19) (2014) 5041–5048 Jun.
[10] S. Wang, I.S. Cole, Q. Li, Toxicity of graphene quantum dots, RSC Adv. 6 (2016) 89867.
[11] L. Xu, Y. Dai, Z. Wang, J. Zhao, J.C. White, B. Xing, Graphene quantum dots in alveolar macrophage: uptake-exocytosis, accumulation in nuclei, nuclear response and DNA cleavage, Part Fibre Toxicol 15 (1) (2018 Nov 13) 45.
[12] C. Wu, C. Wang, T. Han, X. Zhou, S. Guo, J. Zhang, Insight into the cellular internalization and cytotoxicity of graphene quantum dots, Adv Healthc Mater 2 (2013) 1613–1619.
[13] X.Y. Wang, R. Lei, D. Huang, N. Wang, L. Yuan, R.Y. Xiao, L.D. Bai, X. Li, M. Li, X.D. Yang, The permeability and transport mechanism of graphene quantum dots (GQDs) across the biological barrier, Nanoscale 7 (5) (2015) 2034–2041 Feb 7.
[14] D. Wang, L. Zhu, J.F. Chen, L. Dai, Can graphene quantum dots cause DNA damage in cells, Nanoscale 7 (21) (2015) 9894–9901 Jun 7.
[15] R.E. Li, Y.R. Li, H. Zhu, Z. Jia, Graphene quantum dots potently block copper-mediated oxidative DNA damage: implication for cancer intervention, React Oxyg

Species (Apex) 6 (18) (2018 Nov) 406–413.
[16] A.M. Abdelkader, I.A. Kinloch, R.A. Dryfe, High-yield electro-oxidative preparation of graphene oxide, Chem. Commun. (Camb.) 50 (61) (2014 Aug 7) 8402–8404, https://doi.org/10.1039/c4cc03260h.
[17] C.E. Gargett, P.A. Roger, Human endometrial angiogenesis, Reproduction 121 (2) (2001) 181–186 Feb.
[18] D.E. Machado, J.A. Perini, M.M. Orlando, R. Santos-Oliveira, Developing a non-invasive procedure using labeled monoclonal antibody anti-VEGF (bevacizumab) for detection of endometriosis, Biomed. Res. Int. 2015 (2015) 751460.
[19] D.M. Maron, B.N. Ames, Revised methods for the Salmonella mutagenicity test, Mutat. Res. 113 (3–4) (1983) 173–215.
[20] C.F. Araujo-Lima, R.J.M. Nunes, R.M. Carpes, C.A.F. Aiub, I. Felzenszwalb, Pharmacokinetic and toxicological evaluation of a zinc gluconate-based chemical Sterilant using *In Vitro* and *In Silico* approaches, Biomed. Res. Int. 2017 (2017) 5746768.
[21] A. Madni, S. Noreen, I. Magbool, F. Rehman, A. Batoll, P.M. Kashift, M. Rehamn, N. Tahir, M.I. Khan, Graphene-based nanocmposites: synthesis and their theranostic applications, J. Drug Target. 26 (10) (2018 Dec) 858–883.
[22] Shenghai Zhou, Hongbo Xu, Wei Gan, Qunhui Yuan, Graphene quantum dots. Recente progress in preparation and fluorescence sensing application, RSC Adv. 6 (2016) 110775–110788.
[23] S.G. Yim, Y.J. Kim, Y.E. Kang, B.K. Moon, E.S. Jung, S.Y. Yang, Size fraction of fluorescent graphene quantum dots using a cross-flow membrane filtration system, Nanomaterials (Basel) 8 (11) (2018) Nov 21.
[24] J. Peng, W. Gao, B.K. Gupta, Z. Liu, R. Romero-Aburto, L. Ge, L. Song, L.B. Alemany, X. Zhan, G. Gao, S.A. Vithayathil, B.A. Kaipparettu, A.A. Marti, T. Hayashi, J.J. Zhu, P.M. Ajayan, Graphene quantum dots derived from carbono fibers, Nano Lett. 12 (2) (2012) 844–849 Feb 8.
[25] A. Bayat, I. Saievar-Iranizad, Synthesis of green-photoluminescent single layer graphene quantum dots: determination of HOMO and LUMO energy states, J. Lumin. 192 (2017) 180–183.
[26] J. Lin, X. Chen, P. Huang, Graphene-based nanomaterials for bioimgaing, Adv. Drug Deliv. Rev. 105 (Pt B) (2016) 242–254 Oct 1.
[27] M. Longmire, P.L. Choyke, H. Kobayashi, Clearance properties of nano-sized particles and molecules as imaging agents: consideration and caveats, Nanomedicine (Lond) 3 (5) (2008) 703–717 Oct.
[28] S. Fujime, K. Kubota, Dynamic light scattering from dilute suspensions of thin discs and thin rods as limiting forms of cylinder, ellipsoid and ellipsoidal shell of revolution, Biophys. Chem. 23 (1–2) (1985) 1–13.
[29] J. Rodriguez-Fernández, J. Pérez-Juste, L.M. Liz-Marzán, P.R. Lang, Dynamic light scattering of short au rods with low aspect ratios, J. Phys. Chem. 111 (13) (2007) 5020–5025.
[30] X. He, F. Luzi, X. Hao, W. Yang, L. Torre, Z. Xiao, Y. Xie, D. Puglia, Thermal, antioxidant and swelling behaviour of transparent polyvinyl (alcohol) films in presence of hydrophobic citric acid-modified lignin nanoparticles, Int. J. Biol. Macromol. (18) (2019 Jan 30) 35532–35536 pii: S0141-8130.
[31] B. Wang, S. Zhuo, L. Chen, Y. Zhang, Fluorescent graphene quantum dot nanoprobes for the sensitive and selective detection of mercury ions, Spectrochim. Acta A Mol. Biomol. Spectrosc. 131 (2014) 384–387.
[32] O.J. Achadu, I. Uddin, T. Nyokong, Fluorescence behavior of nanoconjugates of graphene quantum dots and zinc phthalocyanines, Photochem Photobiol A Chem 317 (2016) 12–25.
[33] A. Rodallec, S. Benzekry, B. Lacarelle, J. Ciccolini, R. Fanciullino, Pharmacokinetics variability: why nanoparticles are not just magic-bullets in oncology, Crit Rev Oncol Hematol 129 (2018) 1–12 Sep.
[34] S. Vallabhajosula, R.P. Killeen, J.R. Osborne, Altered biodistribution of radiopharmaceuticals: role of radiochemical/pharmaceutical purity, physiological, and pharmacologic factors, Semin. Nucl. Med. 40 (4) (2010) 220–241.
[35] N. Kurantowicz, B. Strojny, E. Sawosz, S. Jaworski, M. Kutwin, M. Grodzik, et al., Biodistribution of a high dose of diamond, graphite, and graphene oxide nanoparticles after multiple intraperitoneal injections in rats, Nanoscale Res. Lett. 10 (1) (2015) 398.
[36] J.R., L.H. Smaje, An analysis of the permeability of a fenestra, Microvasc. Res. 33 (1987) 233–256, https://doi.org/10.1016/0026-2862(87)90020-3.
[37] C. Carrié, S. Rubin, P. Sioniac, D. Breilh, M. Biais, The kinetic glomerular filtration rate is not interchangeable with measured creatinine clearance for prediction of piperacillin underexposure in critically ill patients with augmented renal clearance, Crit. Care 22 (2018) 177.
[38] C. McCallion, J. Burthem, K. Rees-Unwin, A. Golovanov, A. Pluen, Graphene in therapeutics delivery: problems, solutions and future opportunities, Eur. J. Pharm. Biopharm. 104 (2016) 235–350.
[39] H. Sarin, Physiologic upper limits of pore size of different blood capillary types and another perspective on the dual pore theory of microvascular permeability, J. Angiogenes. Res. 2 (2010) 14, https://doi.org/10.1186/2040-2384-2-14.
[40] W. Ren, S. Chen, Y. Liao, et al., Near-infrared fluorescent carbon dots encapsulated liposomes as multifunctional nano-carrier and tracer of the anticancer agent cinobufagin in vivo and in vitro[J], Colloids Surf. B: Biointerfaces 174 (2019) 384–392.
[41] D. Zhang, Z. Zhang, Y. Wu, et al., Systematic evaluation of graphene quantum dot toxicity to male mouse sexual behaviors, reproductive and offspring health[J], Biomaterials 194 (2019) 215–232.
[42] OECD, OECD guideline for testing of chemicals: bacterial reverse mutation test, http://www.oecd-ilibrary.org/environment/test-no-471-bacterial-reverse-mutation-test_9789264071247-en, (1997).
[43] D.E. Levin, M. Hollsetin, M.F. Christman, E.A. Schiwers, B.N. Ames, A new Salmonella tester strain (TA102) with a X T base pairs at the site of mutation detects oxidative mutagens, PNAS 79 (23) (1982) 7445–7449.
[44] A.B. Seabra, A.J. Paula, R. de Lima, O.L. Alves, N. Durán, Nanotoxicity of graphene and graphene oxide, Chem. Res. Toxicol. 27 (2) (2014) 159–168.
[45] G. Storz, M.F. Christman, H. Sies, B.N. Ames, Spontaneous mutagenesis and oxidative damage to DNA in *Salmonella typhimurium*, Proc. Natl. Acad. Sci. U. S. A. 84 (1987) 8917–8921.